Effect of the Air-Water Interface on the Conformation of Amyloid Beta

Suman Samantray and David L. Cheung*

School of Chemistry, National University of Ireland Galway, Galway, H91 TK33, Ireland

Abstract

It has long been recognised that liquid interfaces, such as the air-water interface (AWI) can enhance formation of protein fibrils. This makes liquid interfaces attractive templates for fibril formation but fully realising this requires knowledge of protein behaviour at interfaces, which is currently lacking. To address this molecular dynamics simulation is used to investigate fragments of amyloid beta, a model fibril forming protein, at the air-water interface. At the air-water interface the enrichment of aggregation-prone helical conformations provides a mechanism for the enhancement of fibrillation at interfaces. The conformational ensemble at the air-water interface was also considerably reduced compared to bulk solution, due to the tendency of hydrophobic side chains partitioning into the air restricting the range of conformations. Little overlap between the conformational ensembles at the AWI and in bulk solution was found, suggesting that AWI induces the formation of different set of structures compared to bulk solution. The smaller Aβ(16-22) and Aβ(25-35) fragments show an increase in the propensity for ordered secondary structure at the air-water interface but with a increased propensity for turn over other motifs, illustrating the importance of intra-protein interactions for stabilising helical and extended conformations.

I. INTRODUCTION

The formation of amyloid fibrils, dense linear protein aggregates, is a common feature amongst proteins[1,2]. They first came to prominence due to their connection with a number of diseases[3], such as Alzheimer's, in which the formation of plaques formed by amyloid fibrils was first observed, Parkinson's, and type-II diabetes. Coupled with its implications in disease, fibrils that perform a number of biological functions (functional fibrils) have been identified[4,5]. These functions include formation of structural features, such as biofilms or insect egg cases, information transfer, and the storage of hormones. In many cases functional fibrils take advantage of the excellent material and mechanical properties of protein fibrils. Their properties have also prompted the use of fibrils as components in materials applications. Combining their strength with their biocompatibility has led to a number of applications ranging from biomaterials to electronics.

While amyloid fibrils can form in many environments it has been shown that liquid interfaces, such as air-water or oil-water interfaces, can greatly enhance their formation[6–9]. This is due to a combination of the (i) increased protein concentration at interfaces and (ii) interfaces stabilising conformations favourable for fibril formation[10,11]. Within the body there are a host of interfaces, e.g. cell membrane, surfaces of organelles, that can nucleate fibril formation. This has been implicated in a number of diseases, such as the disruption of membranes by aggregation of islet amyloid polypeptide (IAPP) leading to type-II diabetes[12]. Liquid interfaces have also been used as templates for the formation of ordered structures from a range of building blocks, both synthetic and natural. As such liquid interfaces provide an attractive environment for the formation of fibrils for use in many applications. To realise these applications we need to understand the fibrilliation process at interfaces, in particular understanding how the interfacial conformation of proteins can be related to their fibrillation. Study of the early stages of fibrillation, in particular the conformations adopted by proteins at interfaces will allow us to decouple the effect of the interface templating fibril-favouring conformations and identify intermediate states on the fibrillation pathway.

Investigation of protein conformation at interfaces is challenging experimentally, due to the small length scales involved. Surface sensitive techniques, such as sum frequency generation[13] (SFG), RIME CD[14], and SRCD[15], can give information on molecular structure at surfaces and interfaces. These, however, are ensemble techniques, so are averaged

over all the protein molecules. This is a particular issue for intrinsically disordered proteins (IDPs), such as amyloid beta (Aβ), which lack a well-defined native structure. Understanding the interfacial behaviour of these proteins requires knowledge of the ensemble of different conformations they can exist in and how this is affected by interfaces.

Molecular dynamics simulation has become a powerful tool for the investigation of biomolecular structure. In particular, the use of advanced sampling techniques, such as replica exchange[16] or metadynamics[17], allow for the exhaustive sampling of conformations of IDPs. A number of previous studies have used these to investigate the structure of proteins on interfaces[18–20] and surfaces[21,22], giving new insight into the role of such environments in driving changes to protein structure. In particular for disordered proteins it has been shown that adsorption onto interfaces and surfaces can induce the formation of ordered structures, such as α-helices or β-strands, which may then be prone to further aggregation.

To aid understanding of the fibrillation process it is common to investigate fragments of larger proteins. For Aβ commonly these include the Aβ(10-40) fragment, which lacks the N-terminal region which remains disordered following fibril formation[23], Aβ(16-22) fragment, which contains the central hydrophobic core of the protein, and Aβ(25-35) fragment, which is the smallest fragment to show the same neurotoxic effects of the full protein[24]. While it may be expected that these fragments should mimic that of the full protein, in some cases these can show significantly different behaviour. For instance on gold surfaces the diphenylalanine motif in Aβ(16-22) shows different behaviour to that in the full protein[25,26], which is responsible for contrasting effect of surfaces on the fibrillation of the fragment and full protein. This highlights the importance of larger protein structure on fragment behaviour. To understand this comparison of small and large fragments, in particular investigation of whether the fragment behaves in the same way in a larger molecule than when its on its own, is necessary.

In this paper the behaviour of three fragments of Aβ, Aβ(16-22), Aβ(25-35), and Aβ(10-40), is investigated at the air-water interface (AWI), a model hydrophobic-hydrophilic interface. Comparison with the structures found in bulk solution shows that, in common with studies of other IDPs, the AWI induces the formation of ordered structures. This was primarily α-helical for the largest fragment, significantly different to the structure found in bulk solution. For the smaller two fragments the similar secondary structure motifs were found on both the AWI and in bulk solution but with a higher probability of ordered structure at

the AWI. This difference between the smaller and larger fragment highlights the importance of the larger protein in stabilising secondary structure formation.

II. MODEL AND METHODOLOGY

A. Simulated system

The simulated systems consist of a single protein molecule (Aβ(16-22), Aβ(25-35), or Aβ(10-40) fragment) in water. For Aβ(10-40) and Aβ(25-35)the initial peptide structures were taken from experimental NMR structures (1IYT[27] and 1QYT[28]), with the first nine and last two residues removed for Aβ(10-40). The initial structure for Aβ(16-22) was taken to be a linear chain constructed using Avogadro. Protonation states of the termini and for polarisable residues were set appropriate for pH=7. For the AWI simulations this was placed in a water slab with initial size 80 Å×80 Å×60 Å, 60 Å×60 Å×50 Å, and 60 Å×60 Å×50 Å for Aβ(10-40) Aβ(16-22) and Aβ(25-35) respectively, with the box tripled in the z-direction to give a vacuum layer on each side of the slab. For the bulk simulations the protein was was placed in a cubic water box with side length 70 Å, 40 Å, and 50 Å for Aβ(10-40) Aβ(16-22) and Aβ(25-35) respectively.

B. Simulation method

In order to enhance sampling of protein conformations replica exchange with solute tempering (REST) was employed[29,30]. This is a variation on replica exchange molecular dynamics[31], where the temperature varies only for a subset of the system, in this case the protein. The temperature scaling was performed by scaling the protein-protein and protein-solvent interactions by a factor depending on the effective temperature. Specifically the potential energy was given by[30]

$$E_i = \beta_i E_{pp} + \beta_i^{1/2} E_{ps} + E_{ss} \tag{1}$$

where E_{pp}, E_{ps}, and E_{ss} are the protein-protein, protein-solvent, and solvent-solvent interaction and the scaling factor $\beta_i = T_0/T_i$. For all systems the effective temperature was in the range 300 K to 440 K, slightly wider than used in previous REST simulations of the Aβ(10-40) fragment[32], with the scaling factors and effective temperatures for the different systems

are given in Table I. Exchange attempts between neighbouring replicas were attempted every 500 time steps (1 ps). Transitions between different temperatures and acceptance probabilities are given in the appendix (Figure 8 and Table IV).

		$N_{replica}$	Scaling factors
Aβ(10-40)	AWI	12	1 (300 K), 0.966 (311 K), 0.932 (322 K), 0.9 (333 K), 0.867 (345 K) 0.84 (357 K), 0.811 (370 K), 0.784 (383 K), 0.757 (396 K), 0.731 (410 K) 0.706 (425 K), 0.682 (440 K)
	Solution	10	1 (300 K), 0.956 (313 K), 0.918 (327 K), 0.88 (341 K), 0.843 (355 K) 0.808 (371 K), 0.775 (387 K), 0.742 (404 K), 0.711 (422 K), 0.682 (440 K)
Aβ(16-22)	AWI	6	1 (300 K), 0.926 (324 K), 0.858 (350 K), 0.795 (377 K), 0.736 (408 K), 0.682 (440 K)
	Solution	6	1 (300 K), 0.926 (324 K), 0.858 (350 K), 0.795 (377 K), 0.736 (408 K), 0.682 (440 K)
Aβ(25-35)	AWI	8	1 (300 K), 0.947 (319 K), 0.896 (335 K), 0.849 (354 K) 0.803 (373 K), 0.761 (394 K), 0.72 (417 K), 0.682 (440 K)
	Solution	8	1 (300 K), 0.947 (319 K), 0.896 (335 K), 0.849 (354 K) 0.803 (373 K), 0.761 (394 K), 0.72 (417 K), 0.682 (440 K)

TABLE I. REST scaling factors and effective temperatures.

Interfacial simulations were performed in the NVT-ensemble with the temperature controlled using a velocity rescaling algorithm[33], with a relaxation time of 0.2 ps. Bulk simulations were performed in the NpT-ensemble using the Parrinello-Rahman barostat[34] (relaxation time 2 ps) to control the pressure. All simulations were performed at a temperature of 300 K and the bulk simulations had a pressure of 1 atm. Periodic boundary conditions where used, with a cutoff of 12 Å for the van der Waals and short-range electrostatic interactions. Long-range electrostatic interactions were evaluated using a Particle Mesh Ewald[35] sum with a Fourier spacing of 0.16 nm. Reciprocal space grids of 36×36×36 (bulk solution) and 40×40×160 (surface) were used. The equations of motion were integrated using a timestep of 2 fs, with the LINCS algorithm use to constrain bond lengths[36]. Simulations were performed using the Gromacs simulation package (version 4.6.7)[37–39], using the PLUMED

library[40] to implement REST simulations.

Simulation lengths were 500 ns for the surface simulations and 400 ns for the bulk simulation. Equilibration was judged from considering the number unique conformations found from cluster analysis (Figure 9), with equilibration being achieved once the number of low energy clusters (with free energy within 3 kcal mol^{-1} of the most populated cluster) had plateaued. Following this the simulations were run for a further 200 ns, with analysis performed over this period (unless otherwise stated).

C. Analysis

Analysis of the simulations was performed using a combination of standard Gromacs utilities, custom-written python scripts using the MDAnalysis library[41], and VMD (visual molecular dynamics)[42]. The secondary structure analysis was performed using the STRIDE algorithm[43]. Similarity to helices was also analysed through determining the number of α-helical and 3/10-helical hydrogen bonds[21]

$$N_{\alpha-HB} = \sum_{i=1}^{N_{HB}} \frac{1-(r_i/r_0)^n}{1-(r_i/r_0)^m} \tag{2a}$$

$$N_{3/10-HB} = \sum_{i=1}^{N_{HB}} \frac{1-(r_i/r_0)^n}{1-(r_i/r_0)^m} \tag{2b}$$

where r_0=2.5 Å, n=8, m=12, and the sums run over all potential α-helical (equation 2a) and 3/10-helical (equation 2b) hydrogen bonds, i.e. between backbone carbonyl oxygens and amine hydrogens separated by 4 or 3 residues respectively. The similarity to β-strands was analysed through the dihedral offset function

$$DH = \frac{1}{2}\sum_{i=1}^{N-1} \left(1+\cos\left(\phi_i-\phi_{ref}\right)\right) + \left(1+\cos\left(\psi_i-\psi_{ref}\right)\right). \tag{3}$$

where the sum runs over the ϕ and ψ angles of the protein residues and the reference angles are $\phi_{ref} = -2.36$ rad and $\psi_{ref} = 2.36$ rad, corresponding to an ideal β-strand with alternating residues on opposite sides of the protein backbone.

Protein size was characterised through the radius of gyration

$$R_g^2 = \frac{1}{N}\sum_{i=1}^{N} \left(\boldsymbol{r}_i - \boldsymbol{r}^{com}\right)^2 \tag{4}$$

where $\boldsymbol{r}_i$ is the position of the ith atom and $\boldsymbol{r}^{com}$ is the protein centre of mass and the sum runs over atoms in the protein and the eigenvalues of the gyration tensor

$$G^2_{\alpha\beta} = \frac{1}{N}\sum_{i=1}^{N}(r_{i\alpha} - r^{com}_{\alpha})(r_{\beta} - r^{com}_{\beta}), \alpha, \beta = x, y, z. \tag{5}$$

Formation of compact structures can also be investigated through the number of contacts between Cγ atoms calculated using

$$N_{C\gamma} = \sum_{i}^{N}\sum_{j>i}^{N} f_{switch}(r_{ij}) \tag{6}$$

where the double summation runs over Cγ atoms on different residues and the switching function is given by

$$f_{switch}(r) = \frac{1-(r/r_0)^n}{1-(r/r_0)^m} \tag{7}$$

where $m = 12$, $n = 8$ and $r_0 = 4.5$ Å. Contacts between Cα atoms ($N_{C\gamma}$)are calculated similarly (with $r_0 = 8$ Å). The conformational ensemble was analysed from a cluster analysis, using the method of Daura *et al*[44], using a cut off of 3 Å. Unless otherwise stated analysis was performed for the $\beta = 1$ replica (the only physically relevant one).

III. RESULTS

A. The Air-Water Interface Induces Formation of Helical Structures in Amyloid-β

Adsorption onto the air-water interface significantly changes the structure of Aβ(10-40). The secondary structure (Figure 1(a)) shows large differences between AWI and bulk solution, even from the same α-helical starting structure. At the interface the protein adopts a mixture of conformations, including ones with a high α-helix content. The α-helical conformations typically have two helical regions (V12-D23 and A30-V36). The formation of α-helical structures is consistent with previous experimental studies of Aβ[8,45], which have identified the formation of helical structures that may act as intermediate states for fibrillation on liquid interfaces. In bulk solution, after the initial equilibration period, there are no α-helical conformations. Rather the protein adopts a mixture of β-strand and disordered conformations.

The changes in the protein structure can also be seen from the propensity for different secondary structure motifs (Figure 1(b)). At the AWI regions of higher α-helix propensity

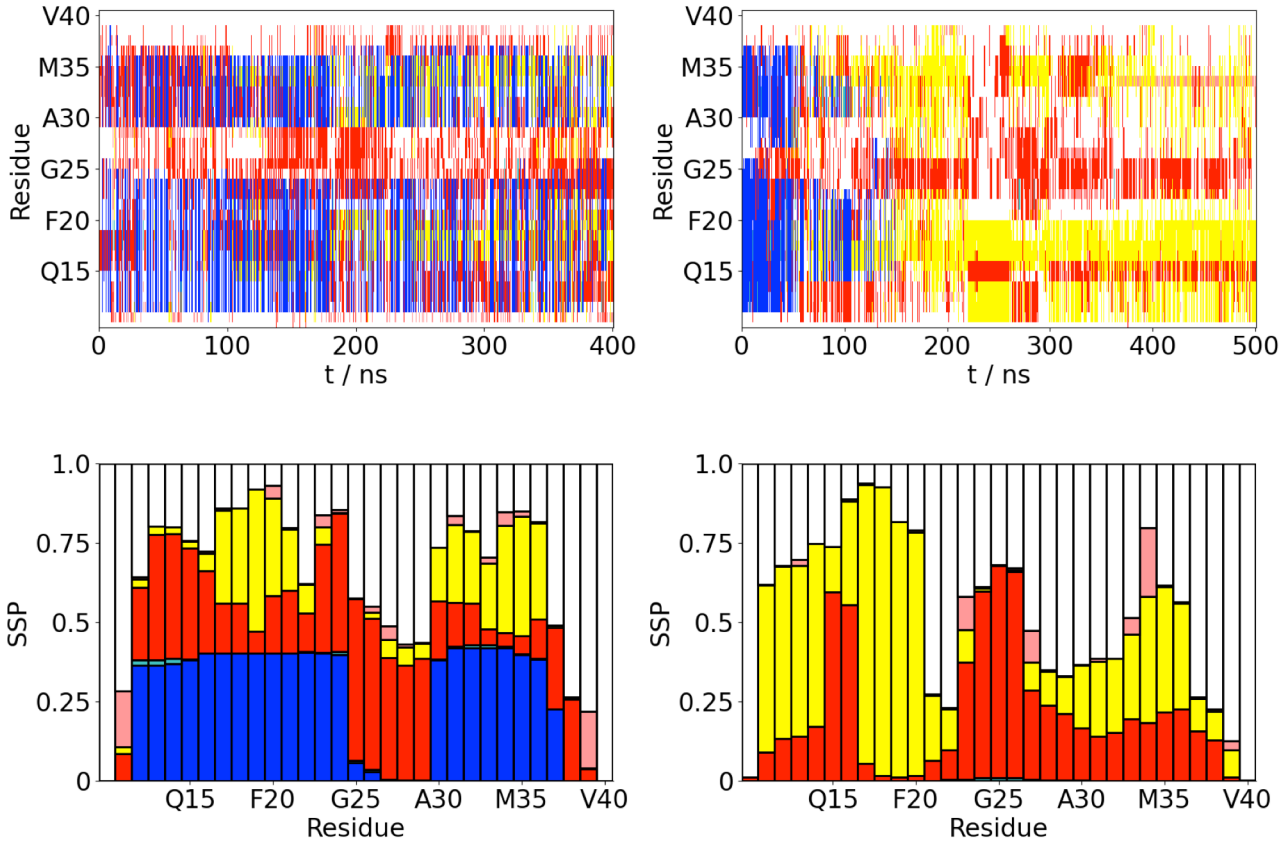

FIG. 1. (a) Time variation of secondary structure for Aβ(10-40) at AWI (left) and in bulk solution (right). α-helix, β-strand, turn, 3/10-helix, and coil denoted by blue, yellow, red, cyan, and white respectively.(b) Secondary structure propensity for each residue (averaged over last 200 ns of simulations). Colours as in (a).

can be seen, consistent with the time series of the secondary structure. Notably no residue has an α-helix propensity above 50 %. There are also some regions (L17-A21 and I31-V36) that have a significant propensity for β-strand formation. These are both contained within the β-strand regions in the Aβ(1-40) fibril[23].

In bulk solution there is a region of high β-strand propensity near the N-terminus (E11-H14 and L17-F20), with the remainder of the protein being less ordered. Notably there is lower propensity for β-strand formation towards the C-terminal end of the peptide. Unlike the AWI there is no α-helical regions.

The tertiary structure of Aβ(10-40) is altered at the AWI (Table II). At the AWI the

protein is slightly more compact, with R_g and G_{max} being larger than in bulk solution. The more compact structure is also evidenced by the higher number of C_α contacts. Notably the number of C_γ contacts is similar in both environments, suggesting that differences in protein structure are reflected largely in the backbone conformation than the packing of the side chains. Consistent with the differences in the secondary structures at the AWI the number of helical hydrogen bonds (both α-helix and 3/10-helix) is higher and the dihedral offset (DH) is lower than in bulk solution.

	AWI	Solution
R_g / Å	10.7±1.6	11.5±1.8
G_{max} / Å	8.9±2.0	9.7±2.1
G_{mid} / Å	5.0±0.7	5.0±0.9
G_{min} / Å	3.4±0.4	3.4±0.4
$N_{C\alpha}$	162±18	148±14
$N_{C\gamma}$	39±6	37±5
$N_{\alpha-HB}$	5.8±6.8	0.5±0.4
N_{3-10}	4.6±3.8	1.5±0.6
DH	36±9	46±2

TABLE II. Structure of Aβ(10-40) at AWI and bulk solution. Quoted uncertainties estimated from standard deviation.

The difference in the secondary and tertiary structure of Aβ(10-40) is driven by the differences in intramolecular interactions, in particular backbone hydrogen bonding, in these environments. Shown in Figure 2 are the probabilities of backbone hydrogen bond formation between the different residues. At the AWI hydrogen bonds consistent with α-helix formation are more probable than in bulk solution, consistent with the higher α-helix propensity (Figure 1(b)). The probability of these hydrogen bonds are <50 %, showing that the α-helical structures are still in a minority. In bulk solution there is a significant probability of hydrogen bonding between the (E11-H14 and L17-F20) β-strand regions, consistent with the formation of an intramolecular anti-parallel beta sheet. Outside of this the hydrogen bond probabilities are typically lower than at the AWI suggesting that a hydrophobic interface induces the formation of more ordered structures.

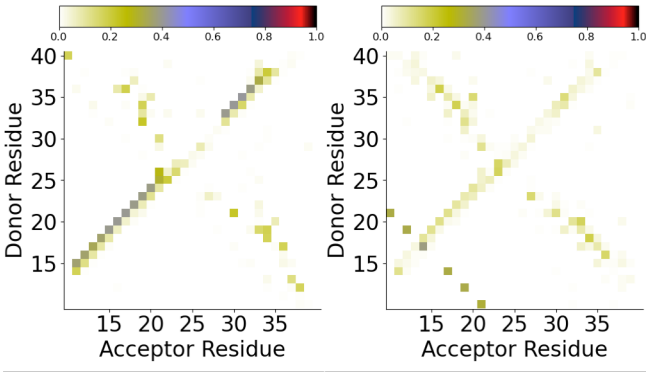

FIG. 2. Backbone hydrogen bond map for Aβ(10-40) at AWI (left) and in bulk solution (right).

The formation of α-helices at hydrophobic interfaces, which has been observed in a number of previous studies[20,46,47], is typically ascribed to the partitioning of hydrophobic residues into the hydrophobic media. Representative simulation snapshots (Figure 3(a)) suggest that this holds for Aβ(10-40). In all cases (for both α-helix and β-strand rich conformations) hydrophobic residues typically lie near the AWI or in the air region.

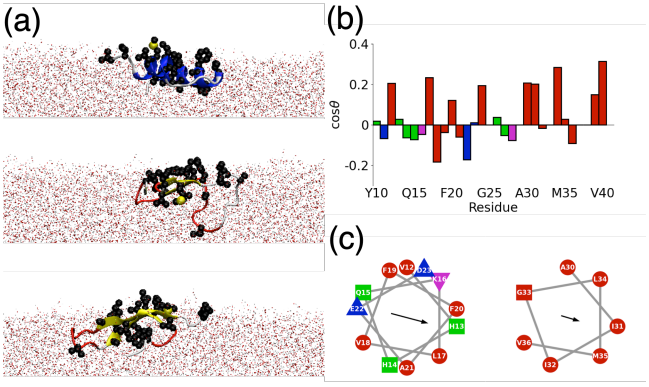

FIG. 3. Aβ(10-40) structure at AWI. (a) Representative simulation snapshots, corresponding to the most common probable structures from cluster analysis. Hydrophobic side chains are highlighted as VDW spheres. (b) Side chain orientation. Red, green, blue, and magenta denote hydrophobic, polar, negatively-charged, and positively charged residues respectively. (c) Helical wheel plots for α-helical regions (V12-D23 and A30-V36). Colours as in (b).

The partitioning of the hydrophobic residues can be assessed quantitively through the orientation of each side chain (Figure 3(b)). Typically hydrophobic residues orient towards

the air-water interface. Consideration of the two principal α-helical regions (Figure 3(c)) shows that in the first of these (V12-D23) forms an amphipathic helix, with a predominately hydrophobic face (consisting of H13, K16, L17, F20, and A21). This hydrophobic face may act as a hotspot for aggregation between neighbouring molecules on the AWI, increasing the rate of fibrillation. The second helical region (A30-V36) is largely hydrophobic (being drawn from the more hydrophobic C-terminus of the protein).

B. Effect of Air-Water Interface on the Conformational Ensemble of Aβ

As an intrinsically disordered protein Aβ exists in an ensemble of different conformations, which can be modified through adsorption onto interfaces. Using cluster analysis the size of the conformational ensemble and typical structures in these different environments can be examined. There is a substantial reduction in the number of distinct conformations at the AWI compared to bulk solution (256 vs 647). This shows that adsorption to the interface restricts the number of conformations the protein can adopt, likely driven by the preferred partitioning of the hydrophobic side chains into air.

Shown in Figure 4(a) are the probability of different clusters for the AWI and bulk solution. While in both environments the first cluster is significantly more probable than the others, it is still < 50 % showing that there is not a single predominant structure in both environments. Despite the reduction in the total numbers of conformations at the AWI, the is decrease in probability with cluster index is slower than in bulk solution. Comparison of the structures of the different clusters (Figure 4(b)) shows that the most common cluster at the AWI is α-helical rich but the other common clusters have a higher β-strand content. This is consistent with the enriched formation of aggregation prone helical intermediates at the AWI. In bulk solution there are no α-helical conformations amongst the most common clusters.

To investigate the difference between the conformational ensembles at the AWI and in bulk solution, the probability of finding each solution-like conformation in the AWI simulation is determined. Following previous work[22] the C_α-C_α distance root mean-squared deviation (DRMSD) is calculated between each saved conformation from the AWI simulation and the clusters found in bulk solution, with the conformations matching if DRMSD$\leq$3 Å. Similar to previous study of the model fibril forming polypeptide hIAPP on hydrophobic

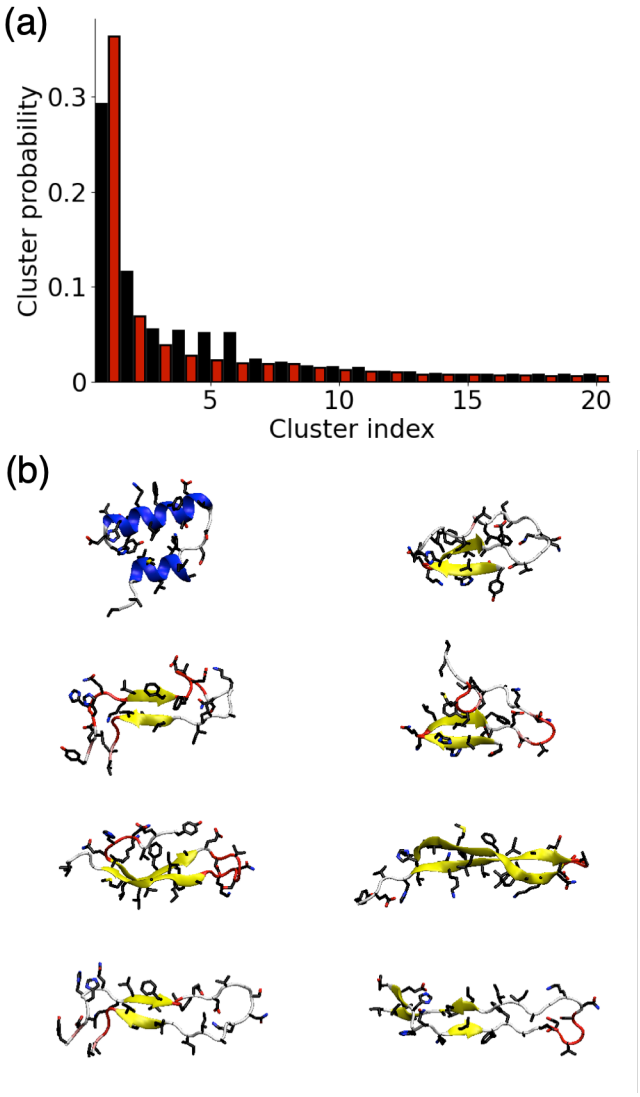

FIG. 4. (a) Probability of different clusters for Aβ(10-40) at AWI (black) and in bulk solution (red). (b) Snapshots showing higher ranked clusters for Aβ(10-40) at AWI (left) and in bulk solution (right).

surfaces, generally the conformations formed at the AWI do not typically correspond to those found in bulk solution, with $\sim$ 66 % of the conformations found at the interface having a DRMSD$>$ 3 Å from any solution conformation. This suggests that the AWI induces the formation of conformations that are qualitatively different to those found in bulk solution. This is similar to behaviour seen for other IDPs on hydrophobic interfaces but differs from the behaviour of Aβ on more hydrophilic gold surfaces[26], suggesting that interfacial hydrophobicity plays a major role in determining the protein conformation. The only solution-like

conformations (Figure 5) that are found with a probability greater than 0.01 correspond to cluster IDs 506 (p = 0.03), 550 (0.02), 571 (0.11), 594 (0.01), and 643 (0.02), where increasing ID corresponds to decreasing probability for these clusters in bulk solution. This indicates that solution-like conformations found at the AWI do not correspond to the most commonly observed conformations in solution. The solution-like clusters typically are either β-strand or random coil, suggesting the the aggregation prone α-helical conformations are induced at the air-water interface and not present in bulk solution.

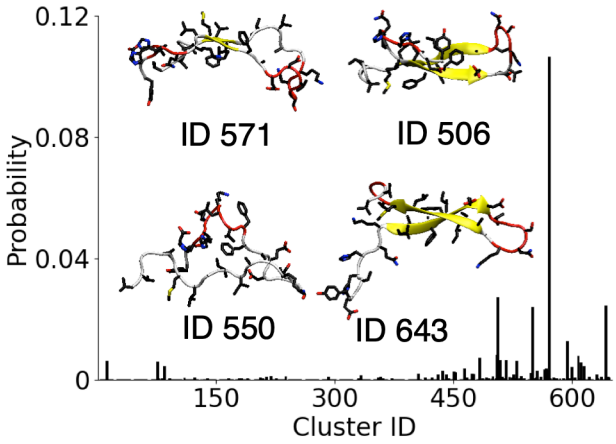

FIG. 5. Probability of Aβ(10-40) solution conformations (by cluster ID) found in AWI simulation. Insets show snapshots of most probable solution-like conformations at AWI.

C. Effects of AWI on Fragment Conformation

Shown in Figure 6 are the secondary structure propensities for the Aβ(16-22) and Aβ(25-35) fragments. Similar to the Aβ(10-40) peptide adsorption at the AWI changes the secondary structure propensity. For both these smaller fragments this is primarily an increase in the proportion of turn residues, caused by an increase in the probability of backbone hydrogen bonding at the AWI. In the Aβ(16-22) the probabilities of the F20-V18 and A21-L17 hydrogen bonds are significantly higher then in solution. For the Aβ(25-35) fragment there is an increase in the probability of L34-I32 hydrogen bonds, increasing the propensity for turn in the second half of the peptide.

Notably for both these fragments the secondary structures are different than in the larger Aβ(10-40) system (Figure 1(b)). Partially this can be attributed to these fragments being

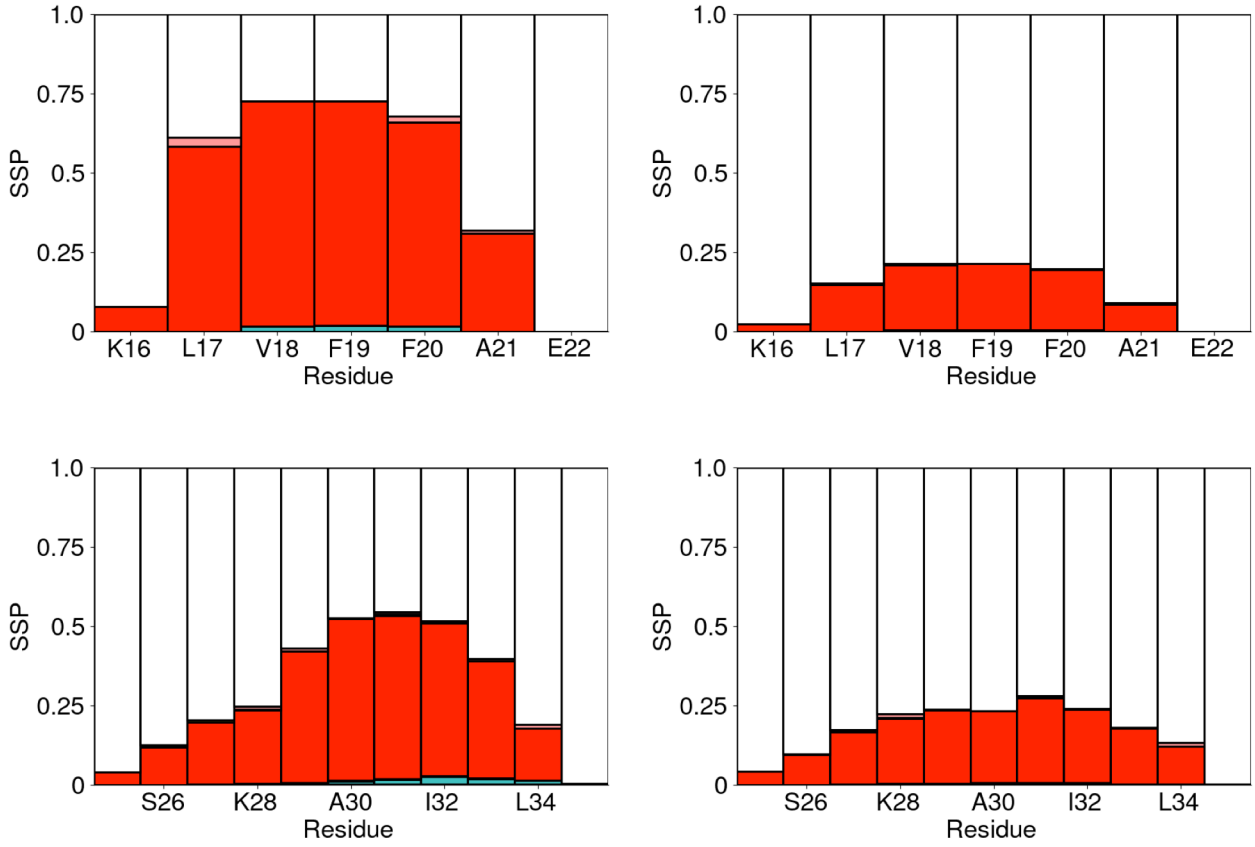

FIG. 6. Secondary structure propensity for each residue (averaged over last 200 ns of simulations) at AWI (left) and in bulk solution (right). Top and bottom show Aβ(16-22) and Aβ(25-35) respectively. Colours as in Figure 1.

too short to sustain helices or strands. For the Aβ(16-22) fragment the most significant structural feature is often considered to be the F19-F20 diphenylalanine motif. Containing two hydrophobic side chains the conformation of this significantly affected by the AWI. Shown in Figure 7 is the probability distribution of the angle between these two sidechains. Compared to bulk solution at the AWI this distribution is shifted towards *cis* states, similar to previous studies of Aβ(16-22) on gold surfaces[25] and the diphenylalanine molecule at the water-cyclohexane interface[48]. This allows both these sidechains to partition into the air, which further stabilises turn conformations. For the larger Aβ(10-40) fragment tendency for *cis* conformations at the AWI is weaker as the adoption of *cis*-states leads to more unfavourable interactions for the rest of the molecule.

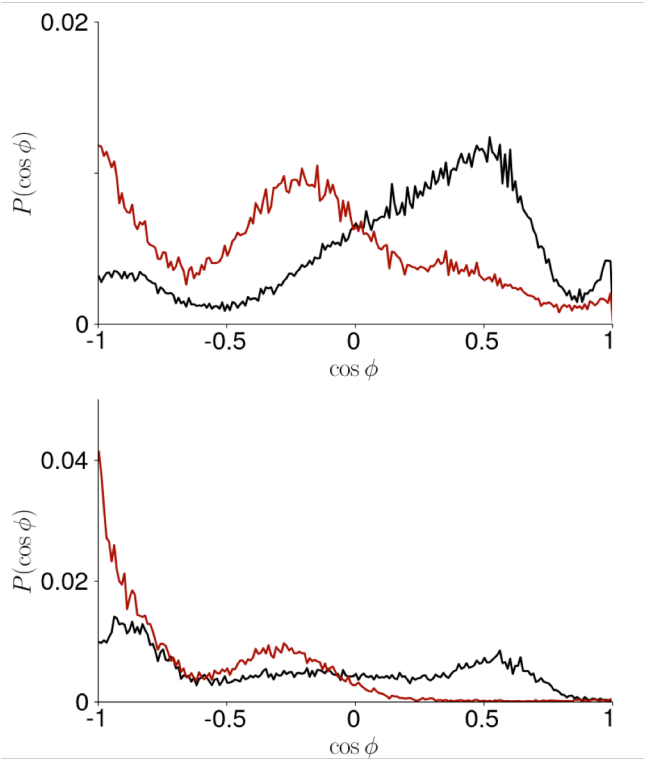

FIG. 7. Histogram of F19-F20 orientation for Aβ(10-40) (top) and Aβ(16-22) (bottom). AWI and solution data shown in black and red respectively.

There is a smaller difference in the secondary structure propensity for the Aβ(25-35)region in the small and large fragments. The first half of this region (G25-G29) is mostly turn (AWI) or random coil (solution) in both cases. Formation of turn, rather than α-helix or β-strand, is due to the lose of interactions that stabilise these structures that are found in the Aβ(10-40) system.

Despite the differences in the secondary structure the tertiary structures of these fragments are similar to the equivalent regions in the (Table III). For both fragments there is a slight decrease in R_g and G_{max}, particularly in bulk solution. The tendency of the AWI to induce more structured conformations may be reducing the differences in tertiary structure between the smaller and larger fragments. Consistent with the loss of helical structures $N_{\alpha-HB}$ and N_{3-10} are both lower for Aβ(16-22) and Aβ(25-35) than for the equivalent regions in Aβ(10-40).

Aβ(16-22)	AWI (frag)	AWI (full)	Solution (frag)	Solution (full)
R_g / Å	5.7±0.4	6.1±0.7	6.6±0.6	7.5±0.4
G_{max} / Å	4.4±0.5	4.9±1.1	5.6±0.9	7.0±0.6
G_{mid} / Å	3.2±0.3	3.2±0.3	3.0±0.4	2.5±0.3
G_{min} / Å	2.2±0.3	2.1±0.4	2.1±0.3	1.9±0.2
$N_{C\alpha}$	17±2	16±3	14±1.5	12.4±0.4
$N_{C\gamma}$	4.6±0.7	3.8±0.6	4.0±0.7	3.2±0.7
$N_{\alpha-HB}$	0.2±0.3	1.0±1.2	0.0±0.1	0±0
N_{3-10}	0.5±0.4	0.8±0.9	0.2±0.2	0.05±0.03
DH	6.8±0.9	6.1±2.4	8.2±1.0	9.4±0.4
Aβ(25-35)	AWI (frag)	AWI (full)	Solution (frag)	Solution (full)
R_g / Å	7.4±1.1	7.4±1.3	8.1±1.2	8.6±0.8
G_{max} / Å	6.3±1.3	6.3±1.4	7.2±1.5	7.3±1.2
G_{mid} / Å	3.5±0.5	3.2±0.5	3.4±0.5	3.8±0.8
G_{min} / Å	2.3±0.3	2.3±0.3	2.2±0.3	2.2±0.2
$N_{C\alpha}$	31±5	32±5	28±4	26±6
$N_{C\gamma}$	4.5±1.1	4.3±1.3	3.7±1.0	3.1±0.6
$N_{\alpha-HB}$	0.2±0.5	1.1±1.2	0.1±0.1	0.05±0.05
N_{3-10}	0.6±0.5	1.1±0.9	0.3±0.3	0.3±0.3
DH	12.2±1.7	11.4±2.3	13.5±1.3	14.0±1.0

TABLE III. Comparison between structures of Aβ(16-22) and Aβ(25-35) fragments and equivalent regions in Aβ(10-40).

IV. CONCLUSIONS

Protein aggregation has long been recognised as being enhanced at liquid (e.g. air-water, oil-water) interfaces. One driving force for this is the interface templating the formation of aggregation-prone conformations. This is particularly true for intrinsically disordered proteins, which typically lack a well defined structure in bulk solution. Using molecular dynamics simulation we found that the model fibril forming protein amyloid-beta can adopt

α-helical conformations at the AWI; this formation of ordered conformations at the AWI is consistent with other IDPs, and contrary to the loss of structure often seen for globular proteins[49].

The formation of helical structures at hydrophobic interfaces has been observed for a number of intrinsically disordered proteins[20,46], suggesting that this is a common feature. Indeed experimental investigation of Aβ[8,45] have identified α-helical intermediates as a key step in its interfacial aggregation. As these helices are commonly amphipathic the exposed hydrophobic faces can make these more prone to aggregation. Notably only one of the two helices formed at the AWI is amphipathic (V12-D23), with the other consisting of solely hydrophobic amino acids.

As an intrinsically disordered protein Aβ exhibits a number of distinct conformations, both at AWI and in bulk solution. The number of conformations is significantly reduced at the AWI compared to bulk solution, due to the partitioning of hydrophobic side chains into the air. There is also little overlap between the sets of conformations in these two environments. This suggests that Aβ exhibits *induced fit*-like[50] behaviour at hydrophobic interfaces, in common with other IDPs.

Comparison between the smaller (Aβ(16-22) and Aβ(25-35)) and larger (Aβ(10-40)) fragments illustrate the influence of the larger protein structure conformational behaviour. Both the smaller fragments show an increase in the propensity for ordered secondary structure, in common with the larger fragment, but for both the smaller fragments this is predominately turn as they are too short to form stable helical or extended structures, at least as monomers. In the case of Aβ(16-22) fragment the difference in secondary structure is further driven by the increased adoption of *cis*-conformations of the F19-F20 diphenylalanine motif at the AWI.

ACKNOWLEDGEMENTS

Computational facilities for this work were provided by the SFI/HEA funded Irish Centre for High End Computing. SS was supported by a postgraduate research scholarship from the College of Science, NUI Galway.

APPENDIX - SIMULATION SAMPLING AND CONVERGENCE

Motion of trajectories between replicas can be monitored through the variation of the REST scaling parameter (β_i) for different replicas (Figure 8)) for Aβ(10-40). As can be seen the replicas explore different values of β_i. Shown in Table IV are the acceptance rates for the simulations. In all cases the acceptance rates are above 20

		0↔1	1↔2	2↔3	3↔4	4↔5	5↔6	6↔7	7↔8	8↔9	9↔10	10↔11
Aβ(10-40)	AWI	0.317	0.331	0.322	0.318	0.324	0.358	0.396	0.352	0.369	0.406	0.345
	Solution	0.246	0.324	0.279	0.238	0.363	0.350	0.334	0.387	0.327		
Aβ(16-22)	AWI	0.330	0.306	0.376	0.337	0.365						
	Solution	0.309	0.293	0.375	0.347	0.378						
Aβ(25-35)	AWI	0.451	0.414	0.490	0.508	0.420	0.498	0.513				
	Solution	0.469	0.451	0.509	0.528	0.466	0.539	0.555				

TABLE IV. Acceptance rates for REST simulations.

To see whether the conformational ensemble has been well sampled the number of unique conformations found (using cluster analysis) against simulation for Aβ(10-40) is shown in Figure 9). As can be seen the number of clusters within 3 kcal mol^{-1} of most common cluster has plateaued within 200 ns for the AWI simulation and 300 ns for bulk solution, suggesting adequate sampling of the conformational ensemble.

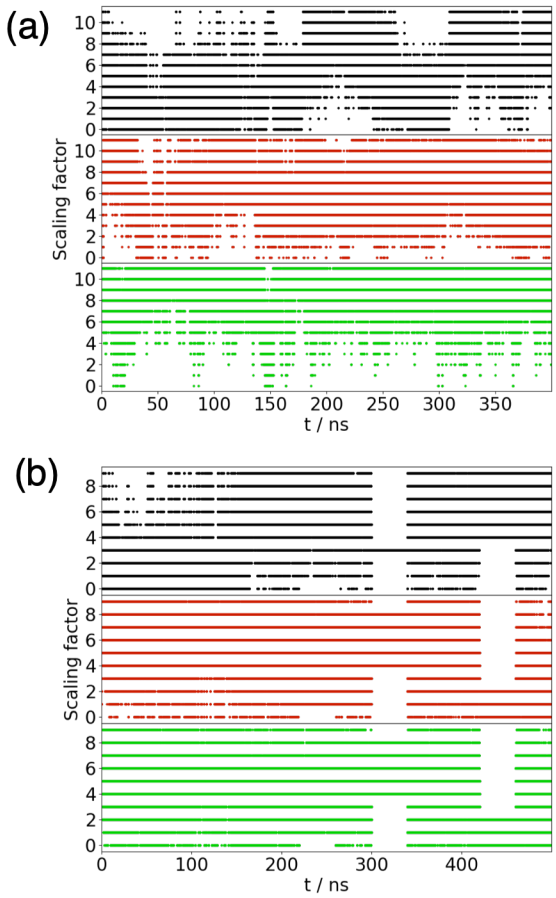

FIG. 8. (a) Plot of scaling factor (i denotes β_i) for Aβ(10-40) at AWI. Graphs show (from top to bottom) replicas with i = 0, 6, and 11 at t=0. (b) Plot of scaling factor (i denotes β_i) for Aβ(10-40) in bulk solution. Graphs show (from top to bottom) replicas with i = 0, 5, and 9 at t=0.

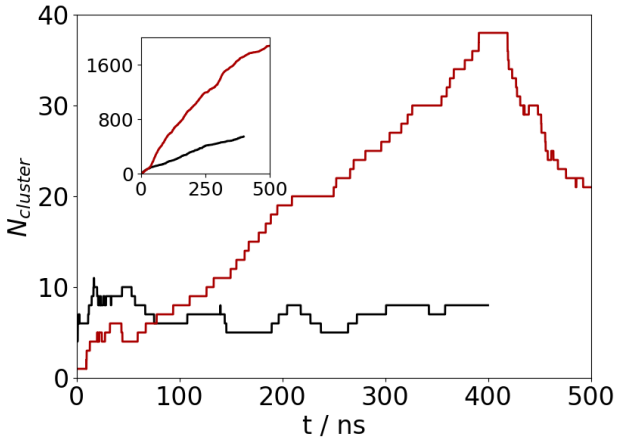

FIG. 9. Number of unique clusters against time for Aβ(10-40) at AWI (black) and in bulk solution (red). Main panel shows number of clustes within 3 kcal mol^{-1} of most common cluster, inset shows total number of clusters.

* david.cheung@nuigalway.ie

[1] F. Chiti and C. M. Dobson, Annual Review of Biochemistry **75**, 333 (2006), ISSN 0066-4154, URL http://www.annualreviews.org/doi/10.1146/annurev.biochem.75.101304.123901.

[2] M. G. Iadanza, M. P. Jackson, E. W. Hewitt, N. A. Ranson, and S. E. Radford, Nat Rev Mol Cell Biol **19**, 755 (2018), ISSN 1471-0072, 1471-0080, URL http://www.nature.com/articles/s41580-018-0060-8.

[3] M. D. Benson, J. N. Buxbaum, D. S. Eisenberg, G. Merlini, M. J. M. Saraiva, Y. Sekijima, J. D. Sipe, and P. Westermark, Amyloid **25**, 215 (2018), ISSN 1350-6129, 1744-2818, URL https://www.tandfonline.com/doi/full/10.1080/13506129.2018.1549825.

[4] T. P. J. Knowles and R. Mezzenga, Advanced Materials **28**, 6546 (2016), ISSN 15214095.

[5] C. Li, R. Qin, R. Liu, S. Miao, and P. Yang, Biomater. Sci. **6**, 462 (2018), ISSN 2047-4830, 2047-4849, URL http://xlink.rsc.org/?DOI=C7BM01124E.

[6] C. Schladitz, E. P. Vieira, H. Hermel, and H. Möhwald, Biophysical Journal **77**, 3305 (1999), ISSN 00063495, URL http://linkinghub.elsevier.com/retrieve/pii/S0006349599771614.

[7] A. Morinaga, K. Hasegawa, R. Nomura, T. Ookoshi, D. Ozawa, Y. Goto, M. Yamada, and H. Naiki, Biochim. Biophys. Acta - Proteins Proteomics **1804**, 986 (2010), ISSN 15709639, URL http://dx.doi.org/10.1016/j.bbapap.2010.01.012.

[8] M. Hoernke, J. A. Falenski, C. Schwieger, B. Koksch, and G. Brezesinski, Langmuir **27**, 14218 (2011).

[9] S. Campioni, G. Carret, S. Jordens, L. Nicoud, R. Mezzenga, and R. Riek, J. Am. Chem. Soc. **136**, 2866 (2013).

[10] L. Jean, C. F. Lee, C. Lee, M. Shaw, and D. J. Vaux, The FASEB Journal **24**, 309 (2010), ISSN 0892-6638, URL http://www.fasebj.org/cgi/doi/10.1096/fj.09-137653.

[11] L. Jean, C. F. Lee, and D. J. Vaux, Biophysical journal **102**, 1154 (2012), ISSN 1542-0086, URL http://www.ncbi.nlm.nih.gov/pubmed/22404938.

[12] N. B. Last, E. Rhoades, and A. D. Miranker, Proceedings of the National Academy of Sciences **108**, 9460 (2011), ISSN 0027-8424, URL http://www.pnas.org/cgi/doi/10.1073/pnas.1102356108.

[13] S. Hosseinpour, S. J. Roeters, M. Bonn, W. Peukert, S. Woutersen, and T. Weidner, Chem. Rev. p. acs.chemrev.9b00410 (2020), ISSN 0009-2665, 1520-6890, URL https://pubs.acs.org/doi/abs/10.1021/acs.chemrev.9b00410.

[14] F. A. Husband, M. J. Garrood, A. R. Mackie, G. R. Burnett, and P. J. Wilde, Journal of Agricultural and Food Chemistry **49**, 859 (2001), ISSN 00218561.

[15] A. J. Miles and B. A. Wallace, Chemical Society reviews **35**, 39 (2006), ISSN 0306-0012.

[16] D. J. Earl and M. W. Deem, Physical Chemistry Chemical Physics **7**, 3910 (2005).

[17] A. Laio and F. L. Gervasio, Rep. Prog. Phys. **71**, 126601 (2008).

[18] D. L. Cheung, Langmuir **32**, 4405 (2016), ISSN 0743-7463, URL http://pubs.acs.org/doi/abs/10.1021/acs.langmuir.5b04619.

[19] D. L. Cheung, Journal of Chemical Physics **147**, 195101 (2017), ISSN 00219606.

[20] D. L. Cheung, J. Chem. Phys. **151**, 064706 (2019), ISSN 0021-9606, 1089-7690, URL http://aip.scitation.org/doi/10.1063/1.5100253.

[21] M. Deighan and J. Pfaendtner, Langmuir **29**, 7999 (2013).

[22] D. L. Cheung, Biointerphases **15**, 051001 (2020).

[23] A. K. Paravastu, R. D. Leapman, W.-m. Yau, and R. Tycko, Proc. Natl. Acad. Sci. **105**, 18349 (2008).

[24] L. Millucci, L. Ghezzi, G. Bernardini, and A. Santucci, Current Protein and Peptide Science **11**, 54 (2010).

[25] L. Bellucci, A. Ardèvol, M. Parrinello, H. Lutz, H. Lu, T. Weidner, and S. Corni, Nanoscale **8**, 8737 (2016), ISSN 2040-3364, 2040-3372, URL http://xlink.rsc.org/?DOI=C6NR01539E.

[26] L. Bellucci, G. Bussi, R. Di Felice, and S. Corni, Nanoscale **9**, 2279 (2017), ISSN 2040-3364, URL http://xlink.rsc.org/?DOI=C6NR06010B.

[27] O. Crescenzi, S. Tomaselli, R. Guerrini, S. Salvadori, A. M. D'Ursi, P. A. Temussi, and D. Picone, European Journal of Biochemistry **269**, 5642 (2002), ISSN 00142956, URL http://doi.wiley.com/10.1046/j.1432-1033.2002.03271.x.

[28] A. M. D'Ursi, M. R. Armenante, R. Guerrini, S. Salvadori, G. Sorrentino, and D. Picone, Journal of medicinal chemistry **47**, 4231 (2004), ISSN 0022-2623.

[29] P. Liu, B. Kim, R. A. Friesner, and B. J. Berne, Proceedings of the National Academy of Sciences of the United States of America **102**, 13749 (2005), ISSN 0027-8424, URL http://www.pnas.org/cgi/content/long/102/39/13749.

[30] L. Wang, R. A. Friesner, and B. J. Berne, Journal of Physical Chemistry B **115**, 9431 (2011), ISSN 15205207.

[31] Y. Sugita and Y. Okamoto, Chemical Physics Letters **314**, 141 (1999), ISSN 1064-3745, URL http://www.ncbi.nlm.nih.gov/pubmed/16957325.

[32] A. K. Smith, C. Lockhart, and D. K. Klimov, Journal of Chemical Theory and Computation **12**, 5201 (2016), ISSN 15499626.

[33] G. Bussi, D. Donadio, and M. Parrinello, Journal of Chemical Physics **126**, 014101/1 (2007), ISSN 00219606.

[34] M. Parrinello and A. Rahman, Journal of Applied Physics **52**, 7182 (1981), ISSN 00218979.

[35] U. Essmann, L. Perera, M. L. Berkowitz, T. Darden, H. Lee, and L. G. Pedersen, Journal of Chemical Physics **103**, 8577 (1995).

[36] B. Hess, H. Bekker, H. J. C. Berendsen, and J. G. E. M. Fraaije, Journal of computational chemistry **18**, 1463 (1997).

[37] D. Van Der Spoel, E. Lindahl, B. Hess, G. Groenhof, A. E. Mark, and H. J. C. Berendsen, Journal of Computational Chemistry **26**, 1701 (2005), ISSN 01928651.

[38] B. Hess, C. Kutzner, D. van der Spoel, and E. Lindahl, J. Chem. Theory Comput. **4**, 435 (2008), ISSN 15499618, URL http://pubs.acs.org/doi/abs/10.1021/ct700301q.

[39] M. J. Abraham, T. Murtola, R. Schulz, S. Páll, J. C. Smith, B. Hess, and E. Lindahl, SoftwareX **1-2**, 19 (2015), ISSN 23527110, URL https://linkinghub.elsevier.com/retrieve/pii/S2352711015000059.

[40] G. A. Tribello, M. Bonomi, D. Branduardi, C. Camilloni, and G. Bussi, Computer Physics Communications **185**, 604 (2014), ISSN 00104655, URL http://dx.doi.org/10.1016/j.cpc.2013.09.018.

[41] N. Michaud-Agrawal, E. J. Denning, T. B. Woolf, and O. Beckstein, Journal of computational chemistry **32**, 2319 (2011), ISSN 1096-987X.

[42] W. Humphrey, A. Dalke, and K. Schulten, Journal of Molecular Graphics **14**, 33 (1996), ISSN 02637855, URL http://dx.doi.org/10.1016/0263-7855(96)00018-5.

[43] M. Heinig and D. Frishman, Nucleic Acids Research **32**, 500 (2004), ISSN 03051048.

[44] X. Daura, K. Gademann, B. Jaun, D. Seebach, W. F. Van Gunsteren, and A. E. Mark, Angew. Chemie Int. Ed. **38**, 236 (1999), ISSN 1433-7851, URL http://doi.wiley.com/10.1002/(SICI)1521-3773(19990115)38:1/2%7B%25%7D3C236::

AID-ANIE236%7B%25%7D3E3.0.CO;2-M.

[45] D. Jiang, K. L. Dinh, T. C. Ruthenburg, Y. Zhang, L. Su, D. P. Land, and F. Zhou, J. Phys. Chem. B **113**, 3160 (2009).

[46] A. De Simone, C. Kitchen, A. H. Kwan, M. Sunde, C. M. Dobson, and D. Frenkel, Proceedings of the National Academy of Sciences of the United States of America **109**, 6951 (2012), ISSN 0027-8424.

[47] C. Dalgicdir, C. Globisch, C. Peter, and M. Sayar, PLOS Computational Biology **11**, e1004328 (2015), ISSN 1553-7358, URL http://dx.plos.org/10.1371/journal.pcbi.1004328.

[48] C. Dalgicdir, O. Sensoy, C. Peter, and M. Sayar, The Journal of chemical physics **139**, 234115 (2013), ISSN 1089-7690, URL http://www.ncbi.nlm.nih.gov/pubmed/24359360.

[49] M. Stefani, International Journal of Molecular Sciences **9**, 2515 (2008), ISSN 14220067.

[50] D. E. Koshland, Proc. Natl. Acad. Sci. **44**, 98 (1958).